SUPPLEMENTARY FIGURE LEGENDS

Supplementary Fig. S1. MIA induces an acute immune response in the fetal brain. (A) Representative images of pSTAT3 staining in sagittal section of the MIA fetal brain. **(B)** Reference atlas for the E12.5 fetal brain. The alterations in pSTAT3 are localized to subpopulations of cells in the prepontine hindbrain (PPH) (green rectangle) and pontine hindbrain (PH) (blue rectangle). **(C)** RNA expression of IL-6 downstream signaling genes in PH laser capture microdissection (LCM) samples. The PH region (arrow) is collected by LCM. Scale bar = 100 μm. MH: medullary hindbrain, TG: trigeminal ganglion.

Supplementary Fig. S2. pSTAT3 staining in the trigeminal ganglion of E12.5 embryos at 3 hours post-poly(I:C) injection. Representative images of pSTAT3 staining in saline and MIA fetal trigeminal ganglion. No overt differences in abundance of $pSTAT3^{+}$ cells are seen in the trigeminal ganglion across fetal brains from saline and MIA. Scale bar = 100 μm. Images are representative of at least 3 independent experiments.

Supplementary Fig. S3. pSTAT3 staining in the medullary hindbrain of E12.5 embryos at 3 hours post-poly(I:C) injection. Representative images of pSTAT3 staining in saline and MIA fetal medullary hindbrain. No obvious differences in pSTAT3 are seen in the medullary hindbrain across fetal brains from saline and MIA. Scale bar = 100 μm. Images are representative of at least 3 independent experiments.

Supplementary Fig. S4. Distribution of IL-6Ra in *Cyp19-Cre^{+};Il6ra$^{fl/fl}$* placenta. Representative images of IL-6Rα staining in the spongiotrophoblast (SP) layer of saline *Il6ra$^{fl/fl}$*, MIA *Il6ra$^{fl/fl}$*, and MIA *Cyp19-Cre^{+};Il6ra$^{fl/fl}$* placentas. Scale bar = 50 μm. Images are representative of at least 3 independent experiments. D: decidua, L: labyrinth, n.s.: not significant.

Supplementary Fig. S5. X-gal staining in brains of wild-type, *Cyp19-Cre*$^{+}$*;ROSA::LSL-lacZ,* and *Ate1*$^{-/-}$ mice. No β-galactosidase is present in adult brains of wild-type and *Cyp19-Cre*$^{+}$*;ROSA::LSL-lacZ* mice, supporting lack of *Cyp19-Cre* directly in the brain. As a positive control, brain of *Ate1*$^{-/-}$ exhibit strong β-galactosidase staining. Images are representative of at least 3 independent experiments.

Supplementary Fig. S6. IL-6Rα staining of adult brains from *Il6ra*$^{fl/fl}$ and *Cyp19-Cre*$^{+}$*;Il6ra*$^{fl/fl}$ offspring. No changes of IL-6Rα^{+} cells in the (upper) Purkinje cells of *Cyp19-Cre*$^{+}$*;Il6ra*$^{fl/fl}$ cerebellum and (lower) motor neurons of *Cyp19-Cre*$^{+}$*;Il6ra*$^{fl/fl}$ motor trigeminal ganglion (MO5), supporting no *Cyp19-Cre* expression in the brain. Arrows indicate IL-6Rα^{+} Purkinje cells. Scale bar = 200 μm. Images are representative of at least 3 independent experiments. ML: molecular layer, GCL: granule cell layer, PCL: Purkinje cell layer.

Supplementary Fig. S7. No gross changes in neuron/astrocyte distribution in the brains of *Cyp19-Cre*$^{+}$*;Il6ra*$^{fl/fl}$ offspring. The neuron/astrocyte distribution is measured by immunostaining with neuronal nuclei (NeuN; black) and glial fibrillary acidic protein (GFAP; red) staining. Images are representative of at least 3 independent experiments.

Supplementary Fig. S8. No body weight differences are found in *Cyp19-Cre*$^{+}$*;Il6ra*$^{fl/fl}$ offspring. Age range for the mice is the age of 3-5 months. 13, 9, 12, 7 adult mice form various litters were used for male *Cre*$^{-}$; male *Cre*$^{+}$; female *Cre*$^{-}$; female *Cre*$^{+}$, respectively. Sex: $F_{(1,37)} = 46.58$, $p < 0.0001$; Cre: $F_{(1,37)} = 3.075$, $p = 0.0878$; MIAxCre: $F_{(1,37)} = 0.06192$, $p = 0.8049$) (Two-way ANOVA). **** $p < 0.0001$ between sex. Data are presented as mean ± SEM.

Supplementary Fig. S9. Cerebellar Purkinje cells are labeled by calbindin (red) and co-stained for glutamic acid decarboxylase-67 (GAD67). There is no obvious difference in GAD67 staining in the PCL between offspring of saline and MIA *Il6ra*$^{fl/fl}$ mice. Scale bar = 200 μm. Images are representative of at least 3 independent experiments. ML: molecular layer, GCL: granule cell layer, PCL: Purkinje cell layer.

Supplementary Fig. S10. Knockout of trophoblast IL-6Rα prevents behavioral abnormalities in both male and female MIA offspring. (A-B) No sex difference was observed in 3 chamber social test. Both male and female MIA *Il6ra*$^{fl/fl}$ offspring showed no preference to mouse (A) chamber and (B) cup, whereas both male and female MIA *Cyp19-Cre*$^{+}$*;Il6ra*$^{fl/fl}$ offspring displayed social preference to mouse (A) chamber and (B) cup. (C-D) No sex difference was observed in marble burying test. (C) In control saline group, no genotype and sex differences were detected in marble burying test. (D) In MIA group, deletion of trophoblast IL-6Rα decreased marble burying behavior in both male and female offspring. * $p < 0.05$, ** $p < 0.01$, *** $p < 0.001$, **** $p < 0.0001$ between groups. Data are presented as mean ± SEM. n.s.: not significant.

Supplementary Fig. S1

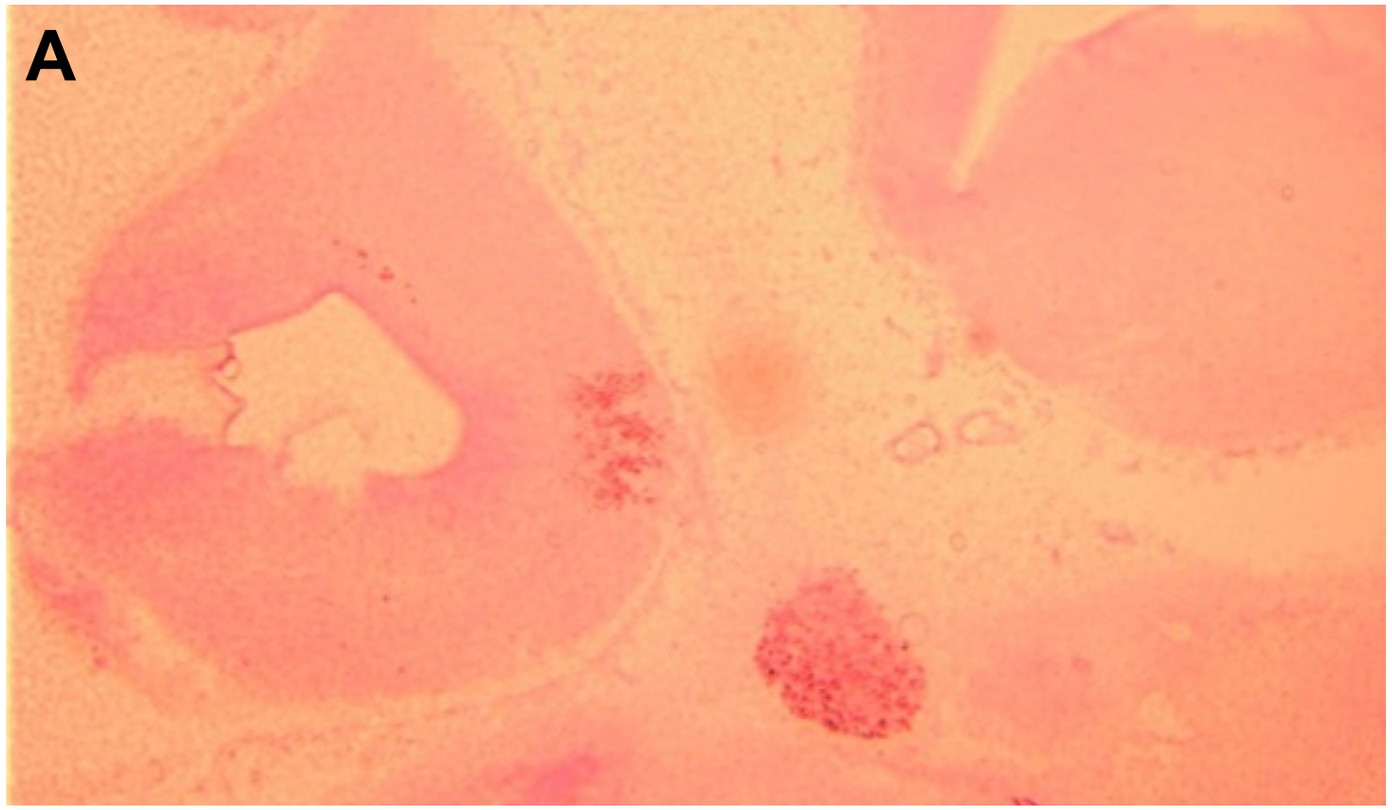

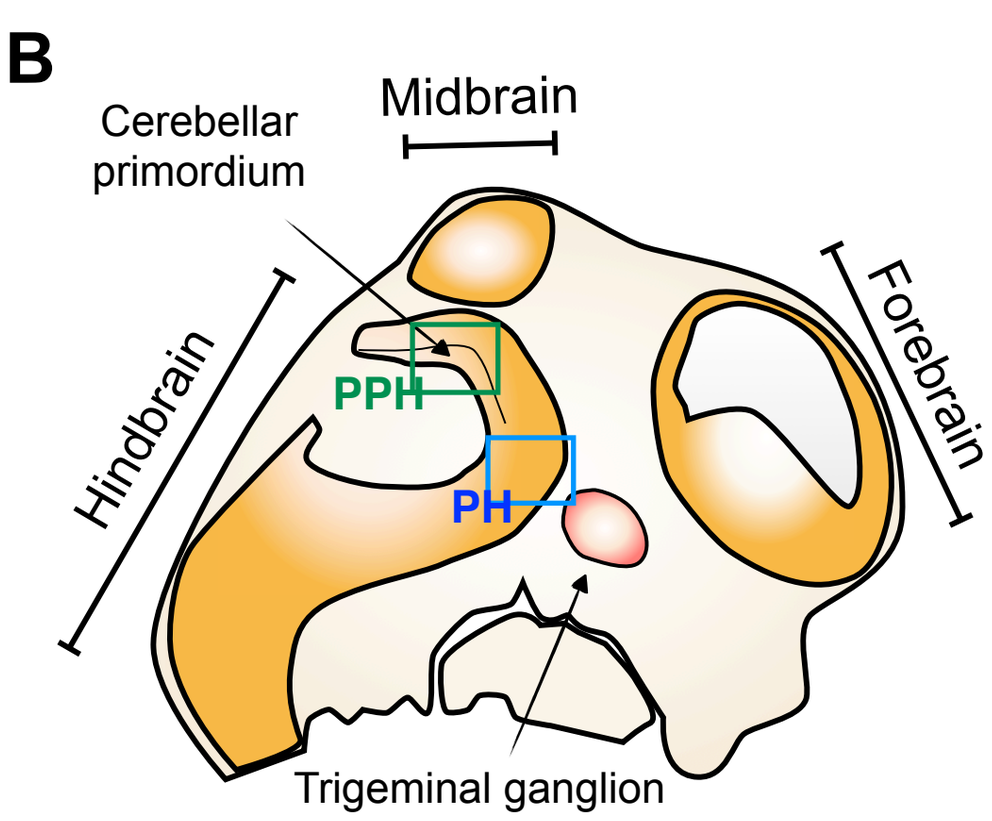

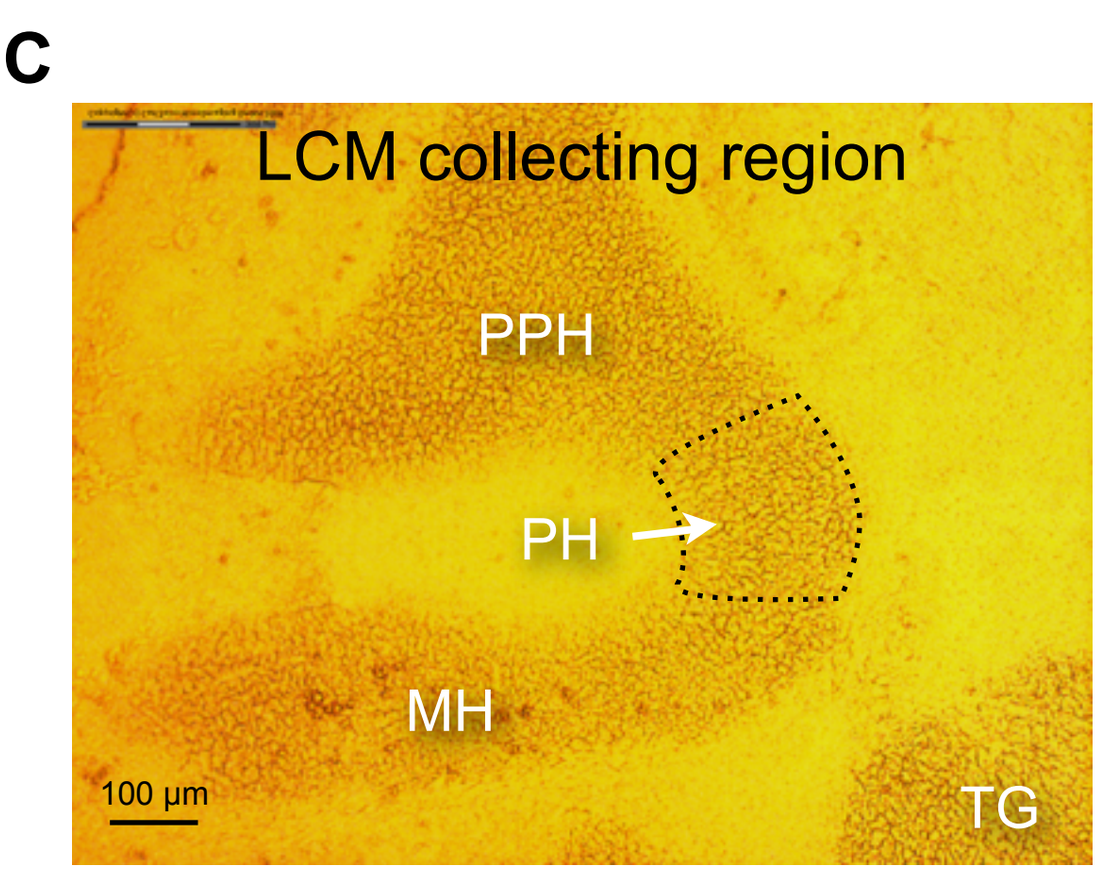

Supplementary Fig. S2

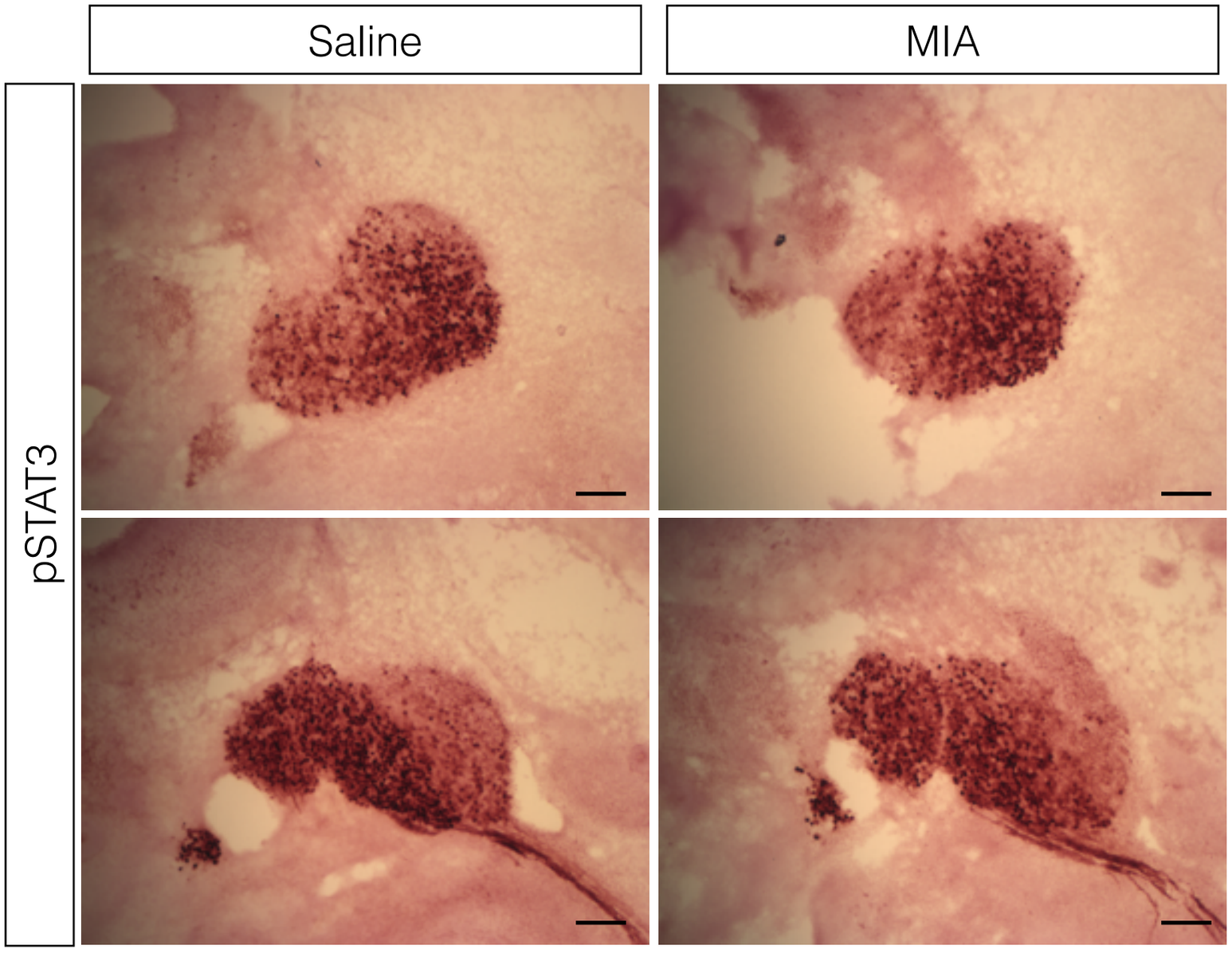

Supplementary Fig. S3

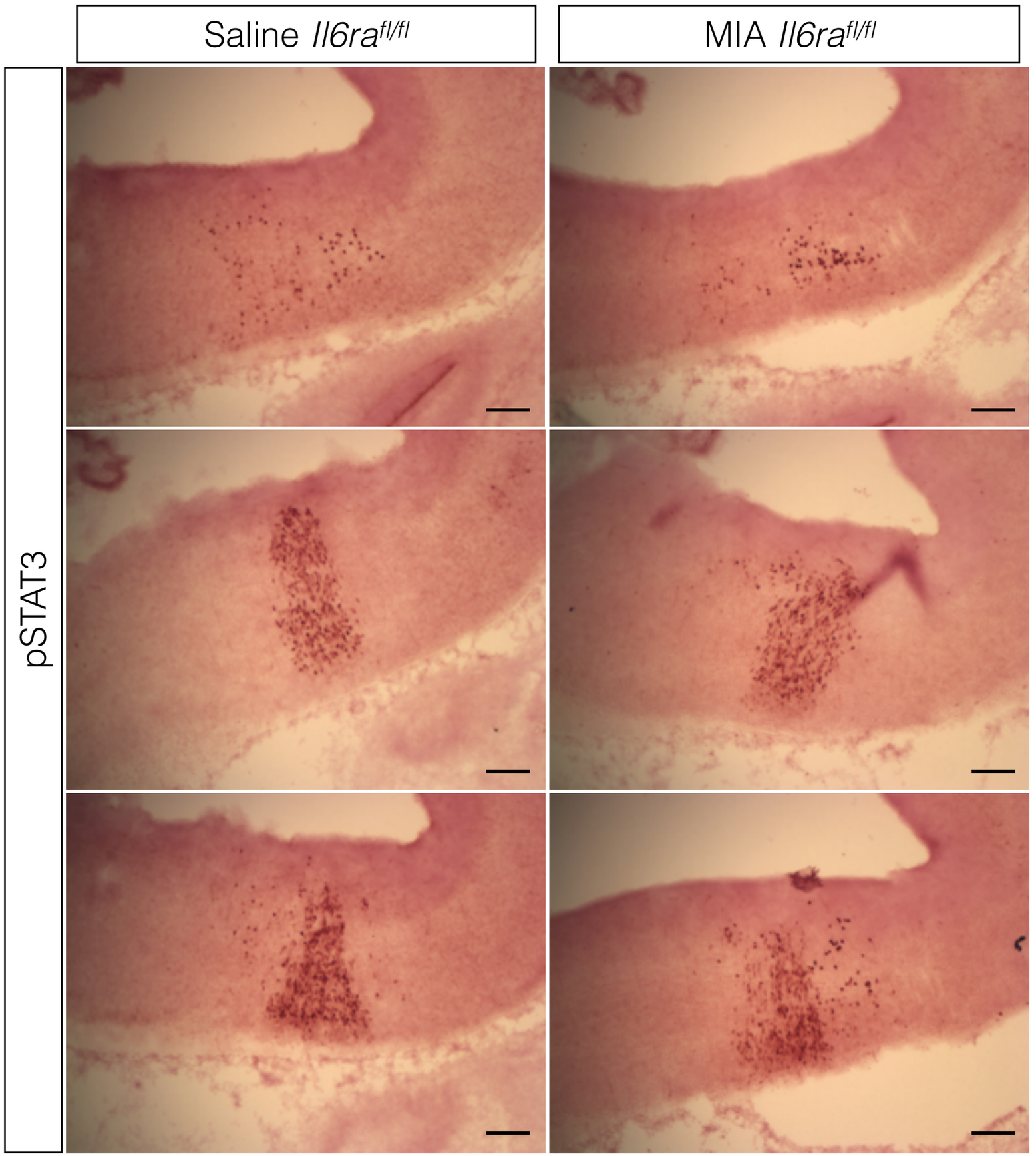

Supplementary Fig. S4

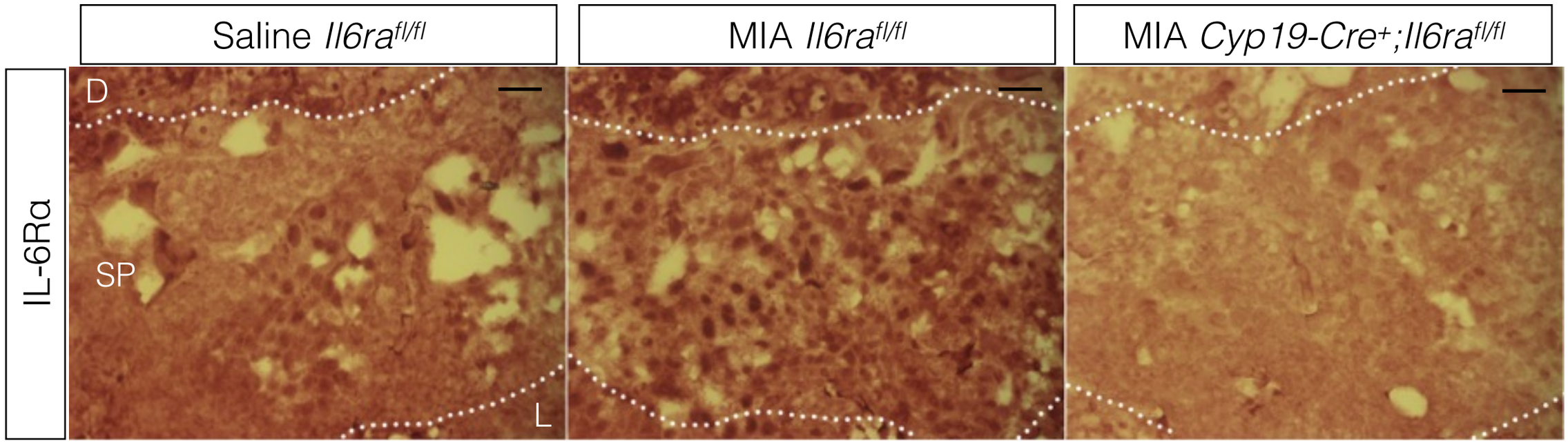

Supplementary Fig. S5

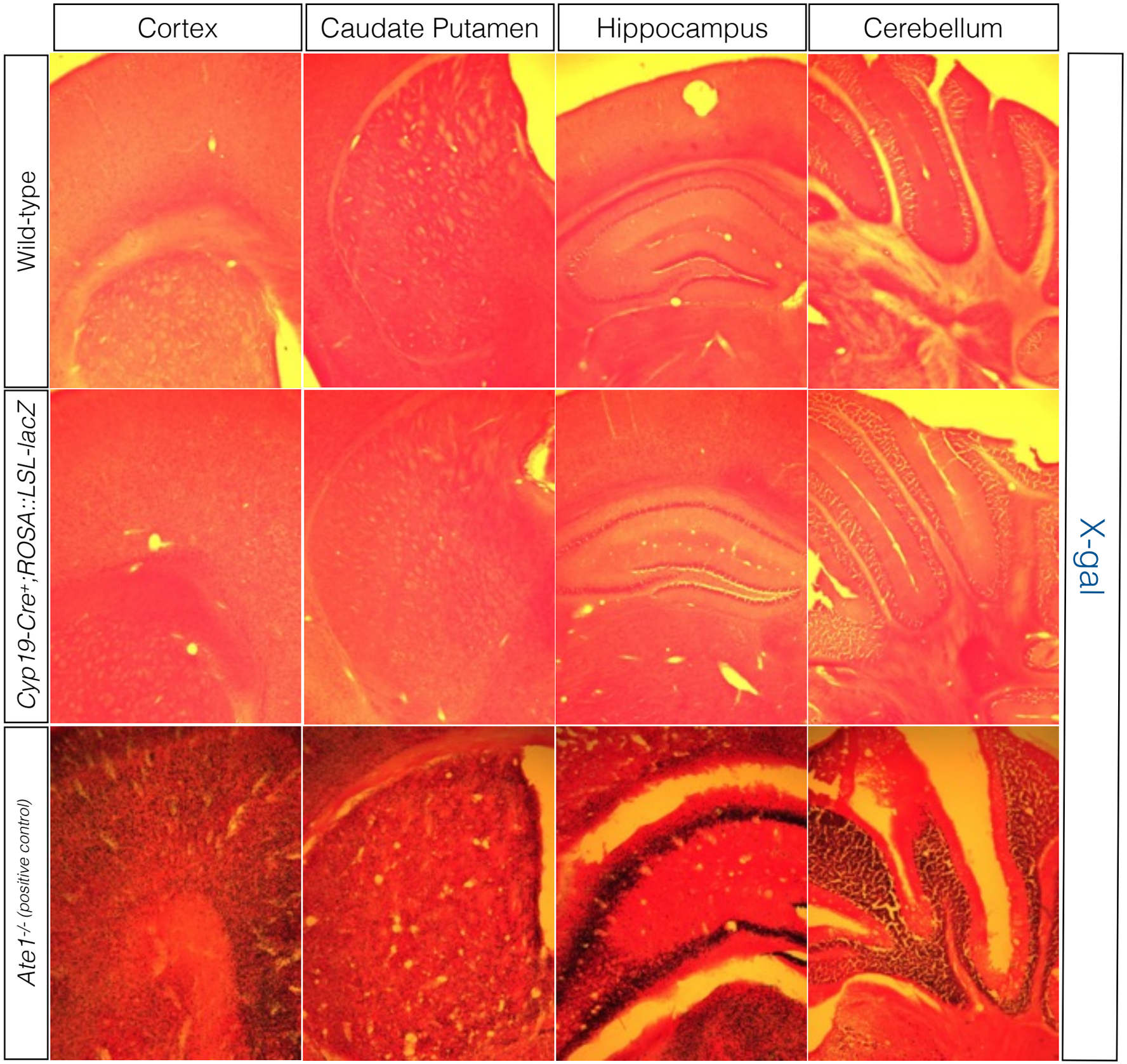

Supplementary Fig. S6

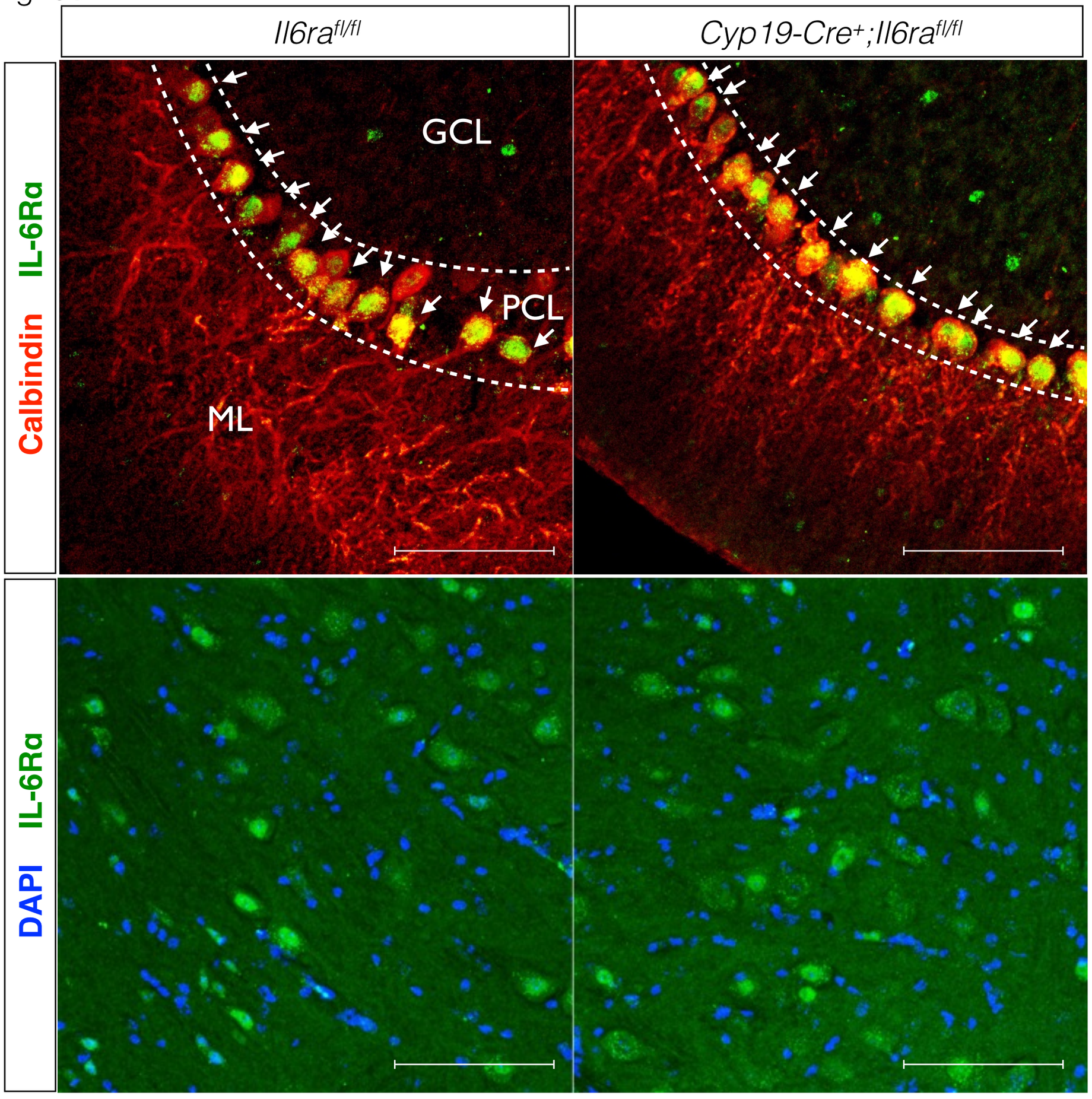

Supplementary Fig. S7

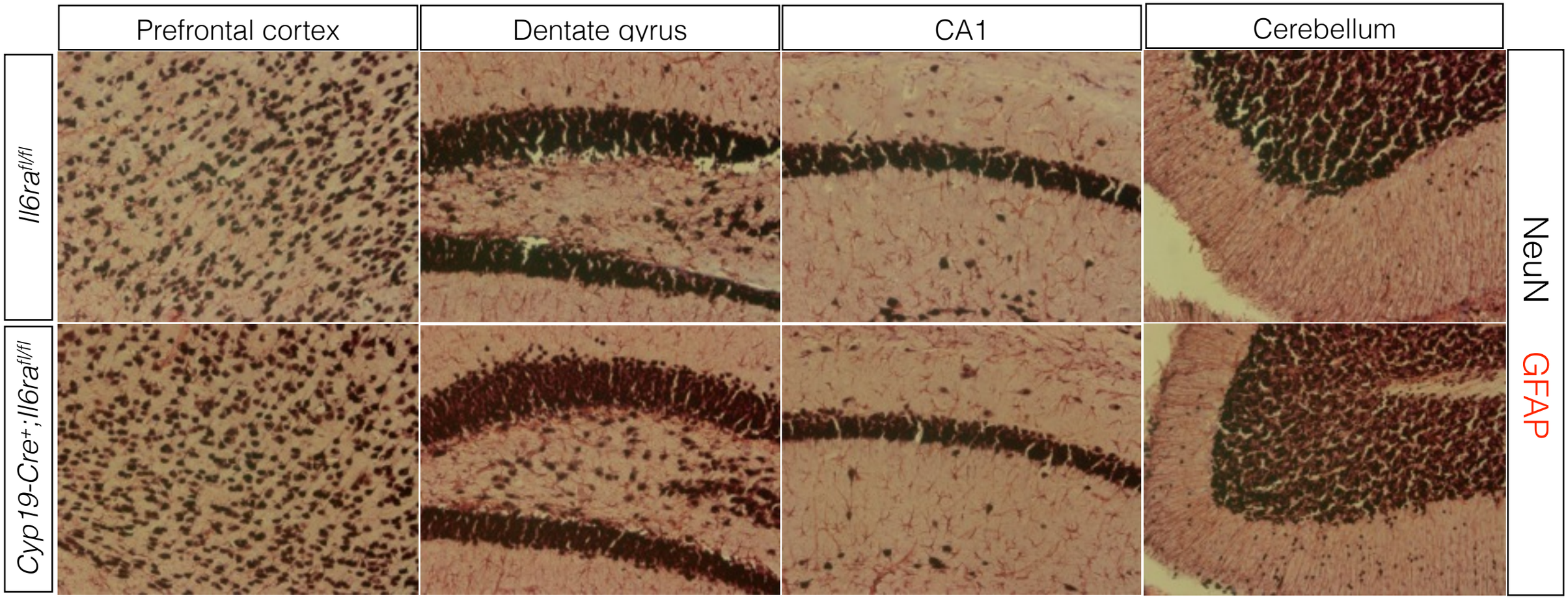

Supplementary Fig. S8

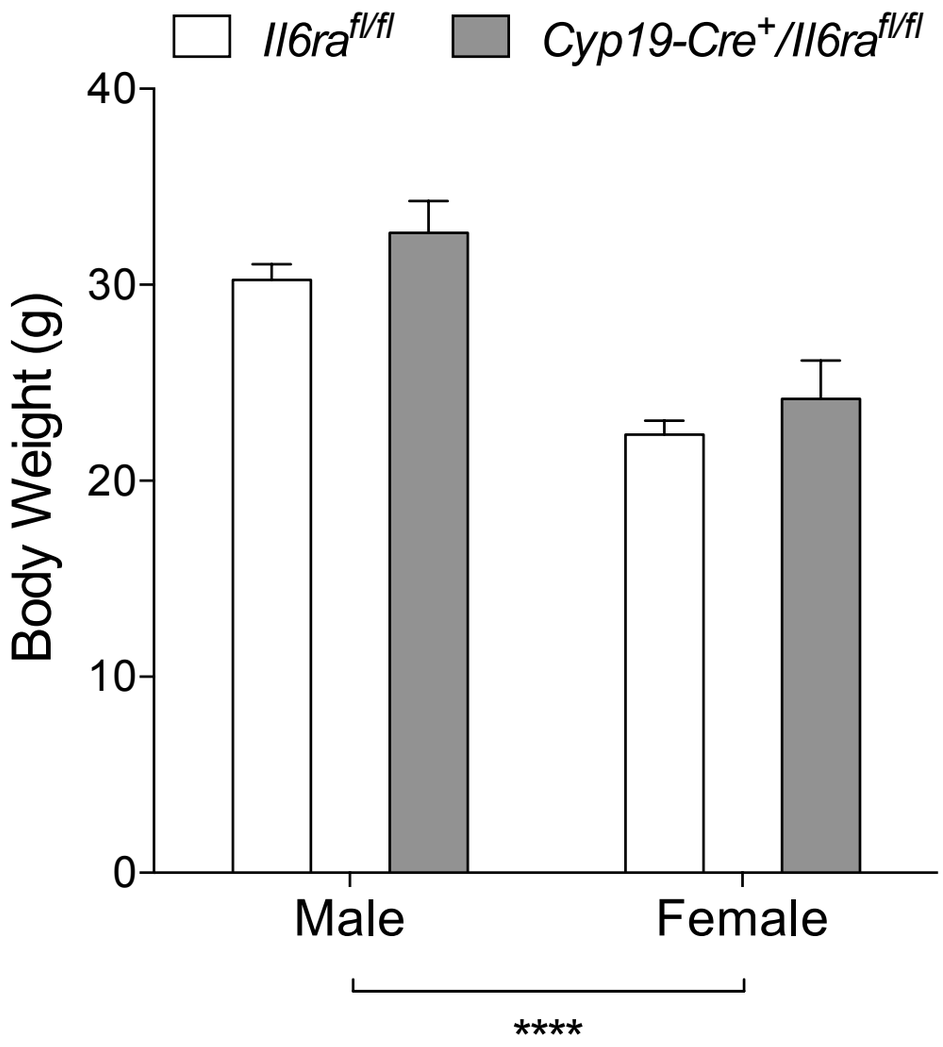

Supplementary Fig. S9

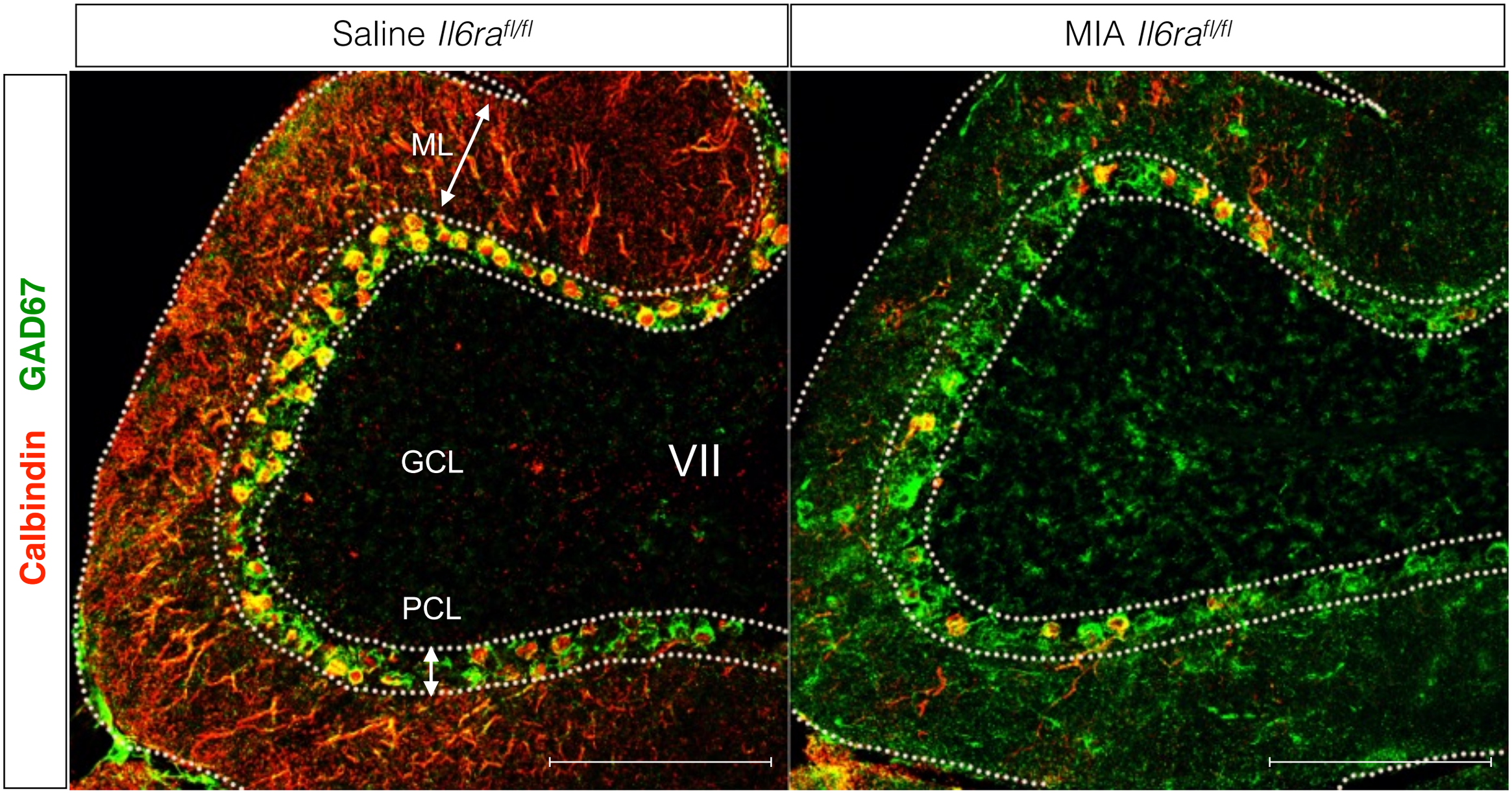

Supplementary Fig. S10